Normal and Reverse Fault Rupture Interaction with Caisson Foundations : Centrifuge Modeling and Numerical Simulation

M. Loli, I. Anastasopoulos

Soil Mechanics Laboratory, National Technical University, Athens, Greece

ABSTRACT: Owing to their rigidity, caisson foundations are believed to be less sensitive to fault induced loading compared to other foundation types. This paper investigates experimentally and numerically the response of a caisson foundation subjected to dip slip (normal and reverse) fault rupture. A series of centrifuge tests were conducted focusing on the effect of the caisson position with reference to the free field fault outcrop. The fault rupture was found to develop preferentially around the margins of the rigid caisson body, which acted as a kinematic constrain, altering sometimes dramatically the free field rupture pattern. Depending on the caisson position, the fault diverted towards the hanging wall or the footwall side of the caisson, or bifurcated, spreading the soil failure at a wider area on both sides. 3-D nonlinear numerical simulation of the problem was also developed and validated through comparison with the experimental results.

1 INTRODUCTION

Although being the generation source of earthquakes, faults were traditionally given little attention by the engineering community. The devastating earthquakes of 1999 in Turkey and Taiwan, however, came to prove that surface fault ruptures can be a significant hazard for structures and highlighted the need to develop design methods and guidelines against faulting-induced loading. A variety of structures were crossed by the surface fault rupture during the Kocaeli (Turkey, 1999) and Chi-Chi (Taiwan, 1999) earthquakes and a significant number of field case histories has been reported in the literature [e.g. Youd et al., 2000; Chang et al., 2000; Dong et al., 2003; Pamuk et al., 2005; Faccioli et al., 2008].

Several studies have considered the response of a structural system interacting with a propagating fault rupture, revealing that the presence of a structure may alter, sometimes dramatically, the free field rupture path. The mechanics of this phenomenon, termed Fault Rupture–Soil–Foundation–Structure Interaction (FR–SFSI), have been analyzed on the basis of : interpretation of real case histories [Anastasopoulos & Gazetas, 2007] ; centrifuge experiments [Bransby et al., 2008; Ahmed & Bransby, 2009] ; and numerical analyses [e.g. Paolucci & Yilmaz, 2008; Anastasopoulos et al., 2008; 2009].

Aiming to extend the research work on the mechanisms of FR–SFSI, which is currently (more or less) limited to the response of shallow foundations, this paper investigates the interaction of deep embedded foundations (caissons) with a rupturing normal and reverse fault. A combination of centrifuge model testing and numerical simulation of the problem was employed to this end. A series of centrifuge experiments were carried out concentrating on the effect of the caisson position relative to the fault. After validating the numerical methodology against experimental results, a parametric study was conducted identifying different interaction mechanisms, taking place for different caisson positions.

2 PROBLEM DEFINITION AND METHODOLOGY

Figure 1 illustrates schematically the main features of the studied problem for the case of normal faulting. A 5 x 5 x 10 (m) square in plan caisson foundation is considered, supported on a 15 m thick layer of dense ($D_r \approx 80\%$) dry sand. It carries a total vertical load of approximately 20 MN, which represents the weight of a superstructure of significant size (e.g., a medium span bridge). Reverse and normal (upwards and downwards) fault displacement of vertical amplitude h (throw) is applied at the bedrock. The displaced block of soil (i.e. the hanging wall) moves with a dip angle of 60°, whereas the footwall remains stationary. The fault deformation forces the caisson to move as a rigid body, experiencing both translational δ and rotational θ displacements.

The location of the caisson relative to the outcropping fault rupture is expressed through parameter s, which is defined as the distance between the caisson right corner and the point that the free-field fault rupture would cross the foundation base. In other words, s indicates the point that the fault rupture would interact with the caisson if fault rupture–caisson interaction did not take place to alter the rupture path. In the following presentation of results s is normalized by the foundation width B.

2.1 *Centrifuge Modeling*

A series of 8 in total centrifuge model tests were conducted in the beam centrifuge of the University of Dundee at an operational acceleration of 100 g. For each type of fault rupture (thrust/normal) a series of 3 fault rupture–caisson interaction tests were conducted, wherein the caisson was placed at different positions relative to the fault s/B, along with an additional free field test, which was used to determine the fault rupture trace in the free field (in absence of the foundation). Table 1 outlines the centrifuge testing program. A photograph of the centrifuge model inside the strongbox is shown in Figure 2a, as deformed after completion of test ML-05, where the caisson was placed at a position $s/B = 0.22$.

The 150 mm deep (i.e. 15 m at prototype scale) soil layer was prepared by dry air pluviation of Fontainebleau sand [Gaudin, 2002]. The sand was pluviated from a specific height with a fixed sieve aperture to control the mass flow rate, giving a uniform density $D_r \approx 80\%$ ($\gamma = 16.11$ kN/m^3). The caisson model was made of steel, having a total mass of 1.025 kg (corresponding to a prototype of 2050 Mg). Aiming to have realistically rough soil–caisson interfaces, the caisson model sides were needle-gunned. A series of direct shear tests were conducted to investigate the soil stress–strain and volumetric behavior as well as the soil–caisson interface frictional properties.

The faulting process was simulated using a split box, the moving part of which is made to translate through a hydraulic actuator. A digital camera was used to take pictures of the model from a fixed position inside the centrifuge "gondola". The photographic data were then analyzed using the Geo-PIV program, written by White et al. [2003], to calculate caisson displacements and the shear strains developed within the soil.

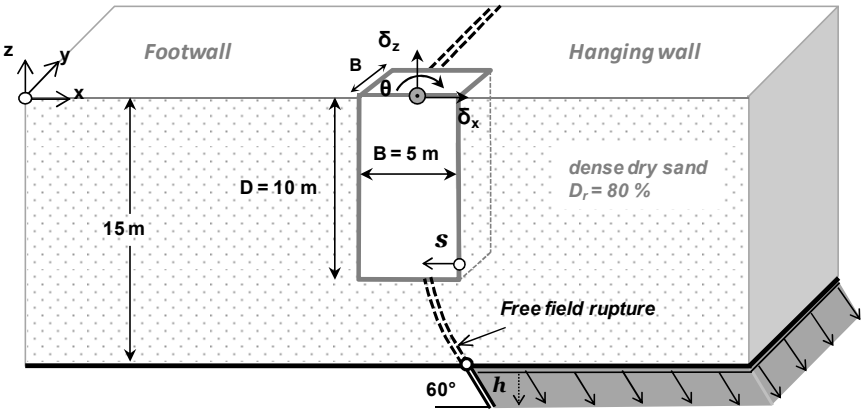

Figure 1. Problem definition : interaction of a rigid caisson with a rupturing normal fault.

Table 1. Centrifuge testing program

Reverse Faults		Normal Faults	
Test	Description	Test	Description
WA-01	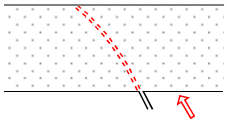	ML-06	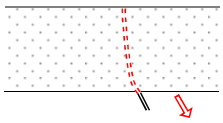
ML-04	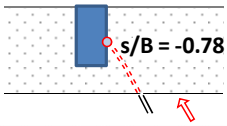	ML-08	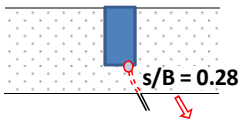
ML-05	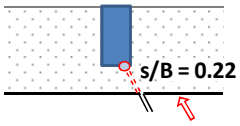	ML-10	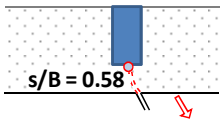
ML-03	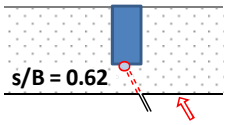	ML-07	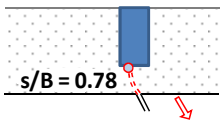

2.2 *Numerical Modeling*

Numerical simulations of the centrifuge model tests were performed employing the finite element code ABAQUS. The model dimensions were chosen to be the same as the dimensions of the physical model at prototype scale and the minimum element width (at the area surrounding the caisson) was set equal to 0.5 m. Figure 2b shows the deformed FE mesh for s/B = 0.22, for comparison with the physical model (Figure 2a). It is noted that only half of the model was simulated, taking advantage of symmetry along the centre-line of the foundation (which corresponds to the location of the Perspex front face in the centrifuge models).

Soil was modeled with hexahedral continuum finite elements. Soil modeling was based on the methodology of Anastasopoulos et al [2007]. An elasto-plastic constitutive relationship was used and encoded in ABAQUS through a user subroutine. This assumes elastic pre-yield soil behavior defined by the secant shear modulus G_s, which was in-creased linearly with soil depth. Failure was defined by the Mohr–Coulomb criterion accompanied with an isotropic strain softening law which degrades the friction (φ) and dilation (ψ) angles linearly with octahedral plastic shear strain. Calibration of the soil model parameters was performed with respect to the results of direct shear tests taking into account the scale effects associated with shear-band modeling.

3-D continuum elements were also used for the caisson, which was assumed to be linearly elastic with typical stiffness properties for steel. The soil–caisson interface was modeled using contact elements to allow sliding and/or detachment to occur. In order to simulate the centrifuge experiments, the interface properties were calibrated to match the frictional properties of the steel–sand interface as measured in the direct shear tests.

3 CHARACTERISTIC RESULTS

Due to space limitations, results are presented in detail only for two of the fault rupture–caisson interaction tests, one for each type of tectonic movement, and compared with the numerical analysis to illustrate the effectiveness of the numerical method. Yet, the mechanisms of fault rupture–caisson interaction for all the studied caisson positions (Table 1) as well as the free field response to reverse and normal fault rupture have been comprehensively reported in Loli et al. [2010 a and b].

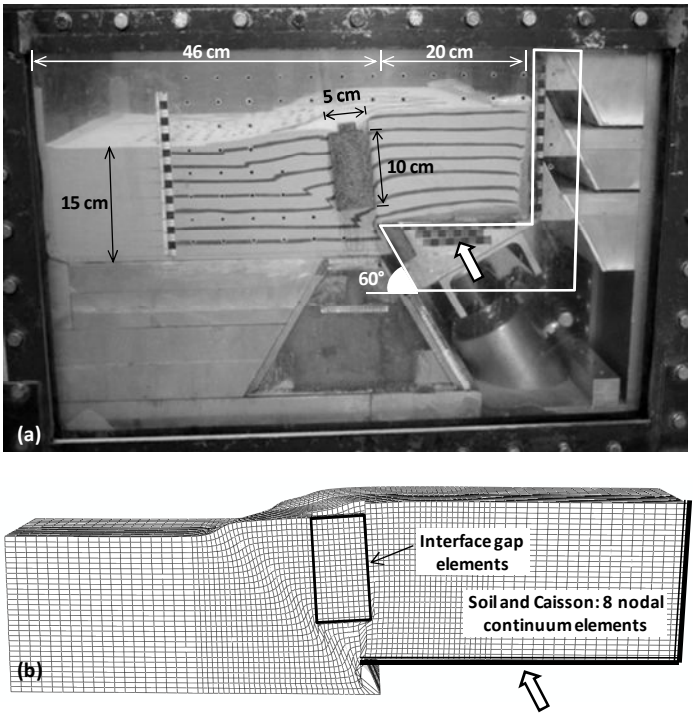

Figure 2. Combined experimental and numerical study : (a) photo of the faulting apparatus and the centrifuge model (for reverse fault rupturing at s/B = 0.22) ; (b) snapshot of deformed FE mesh.

3.1 *Reverse Fault Rupture at s/B = 0.22 (Test ML-05)*

In this test, the caisson was positioned so that the free field rupture would cross the caisson base 1.1 m to the left of its right corner (*s/B* = 0.22). As expected the rigid caisson mass interacts with the rupturing fault modifying significantly the failure pattern in comparison to the free field path. The mechanisms of fault–caisson interaction are highlighted in Figure 3.

Figure 3a shows a set of images captured at different time points during faulting. Significant soil deformation can be observed for h = 0.8 m propagating vertically towards the soil surface on the right (hanging wall) side of the caisson and causing significant sliding to take place along the right caisson sidewall (indicated by the dotted line), yet without evident fault plane formation (see also corresponding shear strain contours in Figure 3b). However, after 0.7 m of additional fault displacement (h = 1.5 m) a localization plane (*F1*) has clearly formed and propagated from the base dislocation point to the right corner of the foundation and all along its right sidewall. At the same time, a secondary localization (*F2*) appears. Initiating from the bedrock dislocation, *F2* intersects with the left (footwall) caisson base corner propagating with a much shallower dip angle. Thereafter, on additional fault displacement, the rupture bifurcates and fault deformation localizes upon these two distinct strands, one at each foundation side. Observe the soil heave formation next to the top right caisson corner due to *F1* and the scarp formed at the soil surface due to the emergence of *F2* for h = 3.5 m.

3.2 *Normal Fault Rupture at s/B = 0.28 (Test ML-08)*

This test, wherein the caisson was subject to normal type fault rupture at $s = 0.28B$, gave the most intriguing fault–caisson interaction mechanisms and subsequently caused the comparatively most intense caisson response (Figure 4).

Figure 4a demonstrates a progressive type of failure associated with the interplay between different failure mechanisms. First, for h = 0.6 m, the caisson acting as a kinematic constraint forces the rupture to deviate significantly from its free field path, actually changing orientation, and to propagate towards the hanging-wall (right) caisson edge. Interestingly, *F1* propagates at a dip angle greater than 90° (about 98°) contradicting the orientation of rupture in the bedrock.

Shear stresses develop along the right sidewall of the caisson and its consequent clockwise rotation causes active type stress conditions to take place on the other (left) side of the caisson. An active failure wedge forms on the footwall side of the foundation for h = 1.0 m, clearly indicated by the respective shear strain contours in Figure 4b. Soil failure on this side, as well as the soil distress underneath the foundation base due to its significant rotation, "facilitate" the diversion of the rupture to the left of the caisson and a secondary rupture plane (*F2*) is mobilized. Thereafter, a rather subtle interaction mechanism is observed, involving the formation of active and passive failure wedges on the left (footwall) and right (hangingwall) side of the caisson respectively, and fault propagation on both sides concurrently (see image for h = 2 m and the equivalent shear strain contours). Moreover, a sliding plane evidently forms along the left sidewall (highlighted in Figure 4a) and a large gap appears at the top left caisson side.

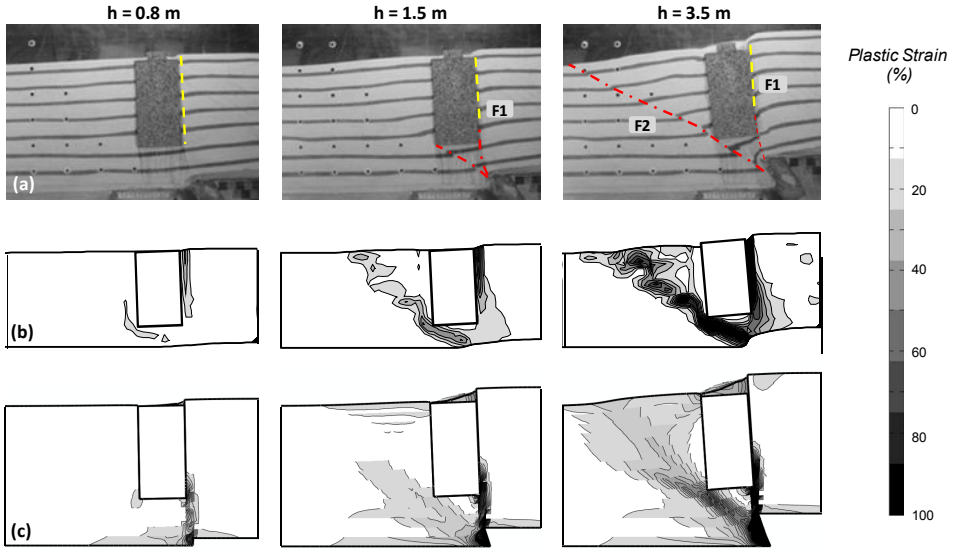

Figure 3. Reverse Fault rupture–caisson interaction at different stages of faulting for s/B = 0.22: (a) centrifuge test images; and contours of shear strains (b) in the centrifuge; (c) in the analysis.

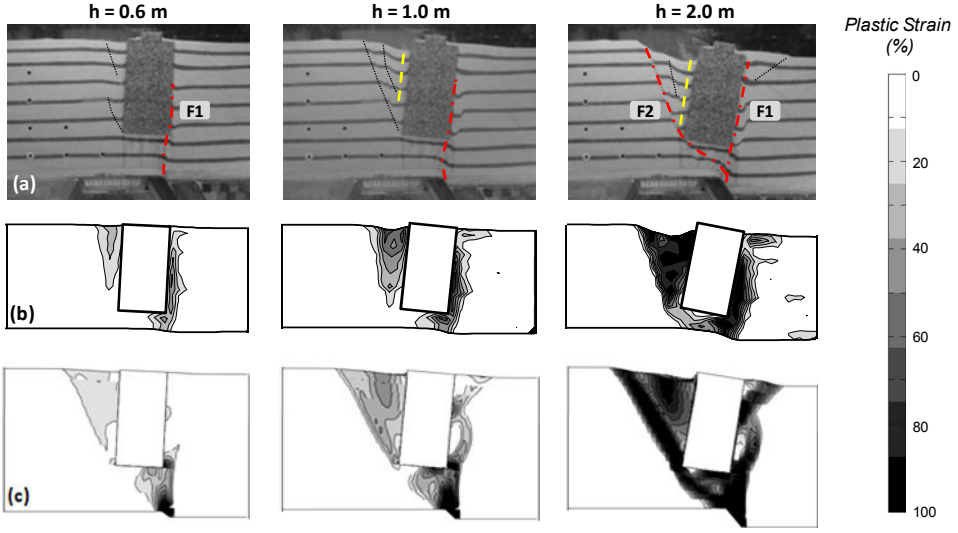

Figure 4. Normal Fault rupture–caisson interaction at different stages of faulting for s/B = 0.28 (Test ML_08): (a) centrifuge test model images; (b) contours of shear strains developed within the soil in the centrifuge test compared to (c) the corresponding numerical analysis.

Comparison between analytically computed and experimentally deduced shear strain contour plots (compare Figure 3b with Figure 3c for reverse faulting and Figures 4b and c for normal faulting) manifests the effectiveness of the numerical method in successfully predicting the generation and evolution of the different fault mechanisms for the whole studied range of fault displacements and for both types of dip-slip faulting. Gaining hence enough confidence in the validity of the numerical method allowed the conduction of a thorough parametric investigation of the exact caisson position effect, which is presented in the following section.

4 EFFECT OF THE RELATIVE TO THE FAULT FOUNDATION POSITION

Figures 5 and 6 summarize the results for reverse and normal faults respectively in terms of the caisson displacements (δx, δz, θ) experienced at different relative fault–caisson positions s/B for different levels of fault throw h. The different failure mechanisms taking place are also indicated by the shear strain finite element contours that correspond to different points (positions) in the graph.

For both types of tectonic movement the plane of caisson response with respect to relative position can be divided into three zones of response A,B, and C, broadly representing three different patterns of fault–caisson interaction mechanism and hence three different modes of foundation response. These are illuminated in the following. To allow comparison with the experiments and show the generally good agreement between analytical and experimental results, centrifuge test results are also indicated (with marker points) for the same fault throws.

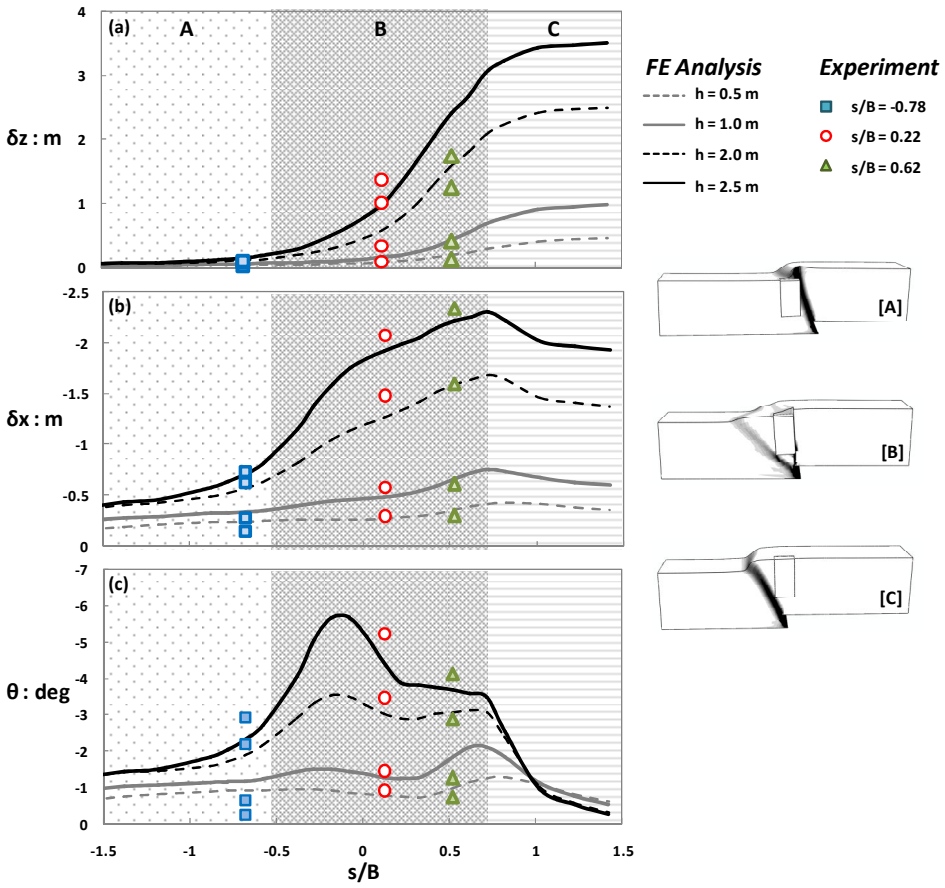

Figure 5. The effect of the exact caisson location (s) on the mechanisms of fault rupture–caisson interaction and the consequent caisson response for the case of *reverse* tectonic movement: (a) vertical displacements, (b) horizontal displacements, and (c) rotation for different levels of fault throw.

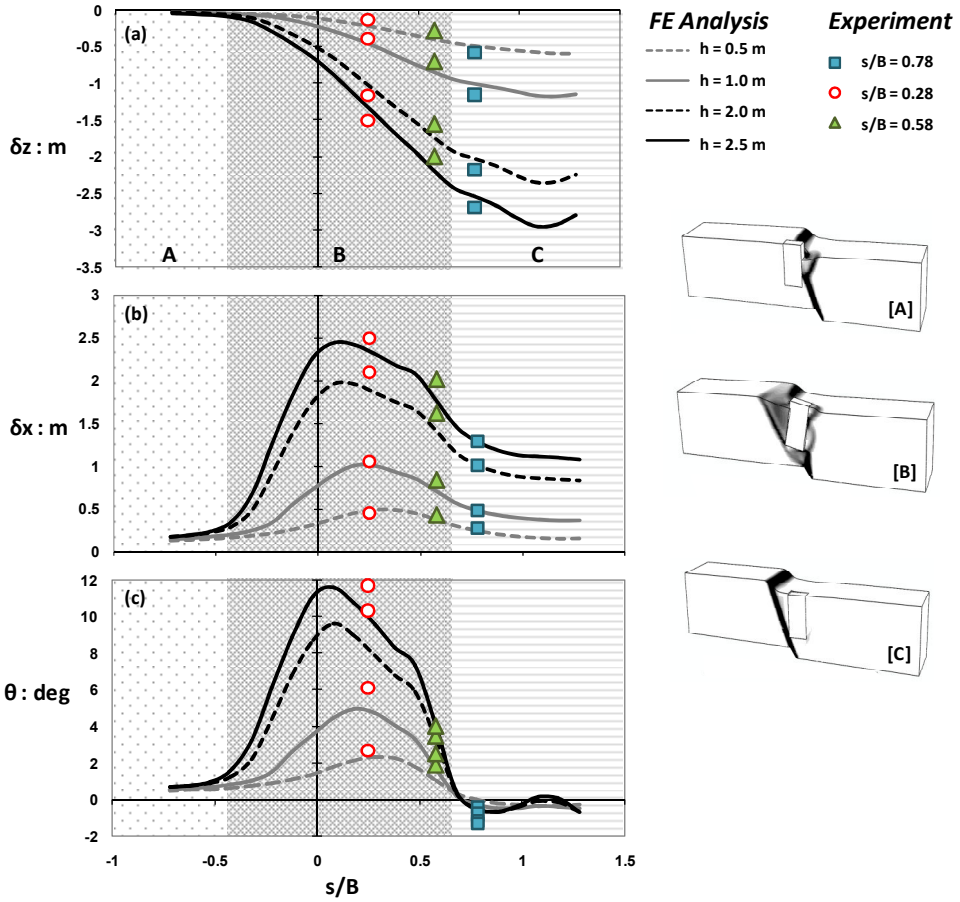

Figure 6. The effect of the exact caisson location (s) on the mechanisms of fault rupture–caisson interaction and the consequent caisson response for the case of *normal* tectonic movement: (a) vertical displacements, (b) horizontal displacements, and (c) rotation for different levels of fault throw.

4.1 *Reverse Fault Rupture–Caisson Interaction Mechanisms*

Three different interaction mechanisms can be identified, dividing the graphs of Figure 5 in three zones : (a) Mechanism A, for $s/B < -0.5$; (b) Mechanism B, for $-0.5 \leq s/B < 0.7$; and (c) Mechanism C, for $s/B \geq 0.7$. More specifically:

Mechanism A is observed when the fault rupture interacts with the upper half of the caisson right sidewall. The rupture is diverted towards the hanging wall and the caisson remains on the footwall. As a result, it experiences limited distress, being subjected to relatively small rotational and horizontal displacement, and practically zero uplift. This zone of s/B is clearly the most favorable for the performance of the supported structure.

Mechanism B occurs when the free field rupture crosses the caisson near its right base corner, as in the case of the previously discussed test ML-05 ($s/B = 0.22$). Fault bifurcation is observed and deformation occurs simultaneously upon two fault strands, one on each side of the caisson. Increased rotations, and hence horizontal displacements, are associated with this zone of response primarily due to the fault deformation spreading within a wider soil area on both sides of the foundation.

Mechanism C (s/B ≥ 0.7; i.e. s > 3.5 m) the fault rupture diverts towards the caisson footwall side, intersecting at its left base corner. This leads to an abrupt decrease of θ, which is virtually eliminated for s/B > 1.0 (i.e. when there is practically no interaction of the fault rupture with the caisson). The caisson experiences pure translational displacement, moving along with the hanging wall.

4.2 *Normal Fault Rupture–Caisson Interaction Mechanisms*

In the same way as with reverse faults, three modes of response can be identified (Figure 6):

Mechanism A ($s/B < -0.4$) takes place when the fault rupture "grazes" the hanging-wall (right) sidewall of the caisson, missing its base by 2 m or more. The rupture path is refracted on the rigid sidewall and deviated towards the hanging-wall (to the right). The caisson remains on the footwall side of the fault, and experiences limited distress for all levels of fault throw h. This is presumably the most favorable area of possible caisson positions.

Mechanism B ($-0.4 \leq s/B < 0.6$) is prevalent when the fault rupture crosses the caisson body near its right base corner. As discussed previously for test ML-08 ($s/B = 0.28$), the interaction of the caisson with the fault rupture is in this case quite complex, involving : (i) bifurcation of the shear zone along both sides of the caisson, (ii) formation of an active failure wedge at the footwall (left) side of the caisson due to its substantial rotation, and (iii) formation of a passive-type failure wedge at the hanging-wall (right) side of the caisson (also due to the rotation). This interaction case, is probably the most detrimental for the system response.

Mechanism C ($s/B \geq 0.6$) prevails when the fault rupture crosses the caisson close to its footwall (left) corner, or misses it completely on the footwall (left) side. The rupture is diverted towards the footwall and the caisson translates downwards, following the hanging wall, with only minor rotation

5 CONCLUSIONS

Caisson foundations interact with dip-slip fault rupture (normal and reverse) and change sometimes dramatically its free field path. The rigid caisson body acts as a kinematic constraint, which forces the fault to divert. This is an important difference of caissons compared to other types of foundations (shallow footings or piles) when the fault can be partially deviated if at all.

A numerical method was developed and validated through successful comparisons with centrifuge test results, revealing its effectiveness in capturing qualitatively and quantitatively the mechanisms of fault rupture–caisson interaction. This gives confidence that the same method can be used to study other similar problems or be used as a design tool.

The validation of the numerical method allowed the conduction of a parametric study to further investigate the effect of the exact foundation position, which proved to be a determinative parameter controlling the response of the system. The different FR-SFSI mechanisms taking place at different positions s/B were identified and the consequent foundation performance was discussed.

6 ACKNOWLEDGMENT

The research presented in this paper was funded by the European Research Council (ERC) Program “IDEAS, Support for Frontier Research – Advanced Grant", under Contract number ERC–2008–AdG 228254–DARE.

7 REFERENCES

Ahmed, W. & Bransby, M.F. (2009). The interaction of shallow foundations with reverse faults. *Journal of Geotechnical and Environmental Engineering*, 135, No. 7, 914-924.

Anastasopoulos, I. & Gazetas G. (2007). Foundation-Structure Systems over a Rupturing Normal Fault: Part I. Observations after the Kocaeli 1999 Earthquake. *Bulletin of Earthquake Engineering*, 5, No. 3, 253–275.

Anastasopoulos, I. Gazetas, G. Bransby, M.F. Davies, M.C.R. & El Nahas, A. (2007). Fault Rupture Propagation through Sand : Finite Element Analysis and Validation through Centrifuge Experiments. *Journal of Geotechnical and Geoenvironmental Engineering*, ASCE, 133, No. 8, 943–958.

Anastasopoulos, I. Gazetas, G. Bransby, M.F. Davies, M.C.R. & El Nahas, A. (2009a). Normal Fault Rupture Interaction with Strip Foundations. *Journal of Geotechnical and Geoenvironmental Engineering*, ASCE, 135, No. 3, 359-370.

Bransby, M.F. Davies, M.C.R. El Nahas, A. & Nagaoka, S. (2008a). Centrifuge modelling of normal fault-foundation interaction. *Bulletin of Earthquake Engineering*, 6, No. 4, 585-605.

Bransby, M.F. Davies, M.C.R. El Nahas, A. & Nagaoka, S. (2008b). Centrifuge modelling of reverse fault-foundation interaction. *Bulletin of Earthquake Engineering*, 6, No. 4, 607-628.

Bray, J.D. Seed, R.B. Cluff, L.S. & Seed, H.B. (1994b). Analysis of earthquake fault rupture propagation through cohesive soil. *Journal of Geotechnical Engineering*, **120**, No. 3, 562-580.

Chang, K-C. Chang, D-W. Tsai, M-H. & Sung, Y-C. (2000). Seismic performance of highway bridges. *Earthquake Engineering and Engineering Seismology*, 2, No. 1, 55-77.

Dong, J.J. Wang, C.D. Lee, C.T. Liao, J.J. & Pan, Y.W. (2003). The influence of surface ruptures on building damage in the 1999 Chi-Chi earthquake: a case study in Fengyuan City. *Engineering Geology*, 71, 157–179.

Faccioli, E. Anastasopoulos, I. Callerio, A. & Gazetas, G. (2008). Case histories of fault–foundation interaction. *Bulletin of Earthquake Engineering*, 6, 557–583.

Gaudin, C. (2002). *Modelisation physique et numerique des ecrans de soutenement: application a l'etude de l'effet d'une surcharge sur le sol soutenu*. PhD. thesis, Universite de Nantes.

Pamuk, A. Kalkan, E. & Ling, H.I. (2005). Structural and geotechnical impacts of surface rupture on highway structures during recent earthquakes in Turkey. *Soil Dynamics & Earthquake Engineering*, 25, No. 7-10, 581-589.

Paolucci, R. & Yilmaz, M.T. (2008). Simplified theoretical approaches to earthquake fault rupture–shallow foundation interaction. *Bulletin of Earthquake Engineering*, 6, No. 4, 629-644.

Ulusay, R. Aydan, O. & Hamada, M. (2002). The behaviour of structures built on active fault zones: examples from the recent earthquakes of Turkey. *Structural Engineering & Earthquake Engineering*, JSCE, 19, No. 2, 149-167.

White, D.J. Take, W.A. & Bolton, M.D. (2003). Soil deformation measurement using particle image velocimetry (PIV) and photogrammetry. *Geotechnique*, 53, No. 7, 619-631.

Youd, T. L. Bardet, J.P. & Bray, J.D. (2000). Kocaeli, Turkey, Earthquake of August 17, 1999 Reconnaissance Report. *Earthquake Spectra*, Suppl. A to 16, 456.